Available online at www.sciencedirect.com
SCIENCE DIRECT®
International Journal of Mass Spectrometry 228 (2003) 613–627
International Journal of Mass Spectrometry
www.elsevier.com/locate/ijms

Reactivity of gaseous protonated ozone: a computational investigation on the carbon monoxide oxidation reaction

Massimiliano Aschi [a,*], Antonio Largo [b]

[a] *Dipartimento di Chimica, Ingegneria Chimica e Materiali, Universita' di L'Aquila, Via Vetoio (Coppito 2), I-67010 L'Aquila, Italy*
[b] *Departamento de Quimica Fisica, Facultad de Ciencias, Universidad de Valladolid, 47005 Valladolid, Spain*

Received 18 November 2002; accepted 20 March 2003

This paper is dedicated to Prof. Helmut Schwarz on the occasion of his 60th birthday.

Abstract

The gaseous protonated ozone has been experimentally observed in FT-ICR conditions to react with carbon monoxide promoting its oxidation to protonated carbon dioxide according to the reaction $HO_3^+ + CO = O_2 + HCO_2^+$. This process, which in the past has been postulated to potentially represent a source of atmospheric ozone depletion, has been computationally addressed in this work. The singlet potential energy surface has been exhaustively investigated at the density functional theory and coupled cluster levels. The picture emerged from the quantum-chemical investigation describes such oxidation process as occurring essentially through a two-step mechanism in which the oxygen and hydrogen atoms are sequentially transferred from protonated ozone to carbon monoxide. By the use of standard statistical kinetics theories, the overall rate constants of the process has been also calculated in a temperature range between 50 and 500 K. Our computational work succeeds in reproducing both the 300 K overall rate constant and the nature of the products.

Keywords: Ozone chemistry; Gas phase ion chemistry; Reactions mechanisms; Multichannel RRKM

1. Introduction

Protonated ozone (HO_3^+) is a key species whose existence has been postulated in a series of crucial atmospheric processes such as the nightime production of $O_2(^1\Delta_g)$ as well as in several oxidation reactions in superacidic medium [1]. Despite its undoubted importance, the difficulties in producing such species made the chemistry of HO_3^+ an essentially unexplored field for a long time. As a matter of the fact, only some theoretical and computational studies did actually appear in the literature [2] remarking, in addition, the difficulties associated to its electronic structure description. Only in the middle 1990s [3] the gaseous HO_3^+ could be generated in the FT-ICR's source and some important thermochemical and reactivity features [4] could be accessed. From such experiments it could be learnt that HO_3^+ does actually reveal a rather variegated chemistry behaving as Brønsted or Lewis acid, depending on the reaction partner.

Particularly interesting turned out to be the oxidation reaction of carbon monoxide [4] formally

* Corresponding author. Tel.: +39-0862-433-775; fax: +39-0862-433-753.
E-mail address: aschi@caspur.it (M. Aschi).

1387-3806/$ – see front matter © 2003 Elsevier Science B.V. All rights reserved.
doi:10.1016/S1387-3806(03)00134-9

characterized by the formal ligand switching process (1)

$$O_2\text{–}HO^+ + CO = O_2 + HO\text{–}CO^+ \quad (1)$$

which was suggested to potentially represent the initial step of the acid-catalyzed ozone depletion process (2) in the upper atmosphere. [5]

$$O_3 + CO = O_2 + CO_2 \quad (2)$$

Interestingly, and fortunately for the environment, despite its exothermicity (vide infra) and the apparently simple S_N2-like mechanism, reaction (1) revealed a rather unefficient process in the low-pressure regime of the FT-ICR experiment resembling the high-atmosphere conditions. An overall bimolecular rate constant equal to 1.2×10^{-10} cm^3 molecule^{-1} s^{-1} was in fact measured with the reactants at 300 K, representing approximately only one-tenth of the average dipole orientation classical capture rate constant [6].

A plausible explanation could be based on the fact that reaction (1) actually shows, as the most exothermic channel at 300 K (unless otherwise stated, all the thermochemical data shown in this work were obtained from [7]), the spin-forbidden route (3)

$$HO_3^+(^1A') + CO(^1\Sigma) = O_2(^3\Sigma_g) + HCO_2^+(^1A') + 85\ \text{kcal mol}^{-1} \quad (3)$$

The HO_3^+/CO system, lacking of heavy nuclei, is therefore unable to efficiently mix the singlet and triplet surfaces. At the same time, reaction (1) could plausibly occurr through the spin-conserving process (4).

$$HO_3^+(^1A') + CO(^1\Sigma) = O_2(^1\Delta_g) + HCO_2^+(^1A') + 57\ \text{kcal mol}^{-1} \quad (4)$$

Such a process, although expected to be strongly favored in the FT-ICR conditions due to its exothermicity and spin-conservation, does not apparently represent a valid alternative to the route (3) for the pluasible presence of high energy barriers along its evolution.

In this paper the details of the singlet hypersurface of the $(CO_4H)^+$ system have been analyzed with the precise aim of trying to propose a quantitative explanation of the low efficiency of the step (4). The implications concerning the reaction (3), i.e., the singlet–triplet surface hopping and all the processes taking place on the triplet surface, are still under investigation in our laboratories and have been disregarded in the present study.

In the first part of the work we outline the features of the $(CO_4H)^+$ potential energy surface (PES). Then, the mechanistic aspects will be addressed on the basis of the resulting PES. Finally, according to the postulated mechanisms, the canonical rate coefficients in vacuo at temperatures ranging from 50 to 500 K will be calculated and compared to the available experimental results.

2. Computational details

The geometries of the different species on the $(CO_4H)^+$ surface have been optimized using density functional theory (DFT). In particular we employed Becke's three-parameter exchange functional [8] and the correlation functional of Lee–Yang–Parr [9], a conjunction that is usually denoted as B3LYP. Dunning's correlation-consistent basis sets cc-pVDZ and cc-pVTZ [10,11], of double-zeta and triple-zeta quality, respectively, were employed for the geometry optimizations. Harmonic vibrational frequencies have been computed on each optimized structure at its corresponding level of theory. This allows an assessment of the nature of stationary points and also serves to estimate the zero-point vibrational energy (ZPVE) correction.

In order to refine the electronic energies we have carried out B3LYP calculations with the aug-cc-pVTZ basis set, which includes diffuse functions that may be important for positively-charged species. In addition we have also performed single-point calculations on the B3LYP/cc-pVTZ geometries with the CCSD(T) method [12] (coupled-cluster single and double excitation model augmented with a non-iterative triple excitation correction) with the cc-pVTZ basis set.

All quantum-mechanical calculations reported in this work were carried out with the Gaussian 98 program package [13].

The 300 K thermochemical quantities were calculated using standard statistical mechanics formula in the ideal gas approximation for obtaining the $C_v(T)$ values.

The global rate coefficients were evaluated in the framework of the statistical theories [14]. All the unimolecular steps along the path were treated using standard RRKM approaches at a fixed energy and total angular momentum J considering K as an active rotor [15]. For barrierless reactions the actual locations of transition structures were carried out with two different approaches both based on the variational determination of the sum of the states calculated along the minimum energy path at fixed energy and total angular momentum. The first approach, hereafter called as reaction path-based (RP) [14], basically describes all the oscillators orthogonal [16] to the reaction path in the harmonic approximation and none of them is treated as a transitional mode, i.e., none of them is supposed to switch to a free-rotor motion. In the second approach the transitional and conserved modes are decoupled and the sum of the states is evaluated through a convolution of a classical phase-space-integral-based evaluation of the transitional modes and of a direct quantum sum for the conserved ones. The algorithm employed at this end, which basically performs a Monte Carlo phase-space integration, is based on the variable reaction coordinate-transition state theory (VRC-TST) [17] implemented in the program VARIFLEX [18]. The microcanonical overall rate constants are finally averaged in the ideal gas approximation, i.e., the Boltzmann distribution, in order to obtain the overall $k(T)$. With the only exception of the VRC-TST calculations, all the RRKM and variational-RRKM calculations were performed with our own routines in which the sum and density of the states were calculated using the Steepest Descent algorithm [19]. At this end all the harmonic frequencies showing vibrational temperatures much lower than the actual temperature of averaging (see below) were considered as free rotors with a rotational constant equal to $\nu^2/(2k)$, where ν is the associated harmonic frequency as k is the force constant. The tunneling correction was taken into account by means of the monodimensional generalized Eckart potential [20].

3. Results and discussion

3.1. Outline of the potential energy surface

The prediction of geometrical parameters for HO_3^+ at the B3LYP/cc-pVTZ level are in reasonable agreement with other previous theoretical works [21] on this species which employed more expensive methods. Schaefer and coworkers [2b] performed a rather complete study on the different plausible HO_3^+ isomers at the CCSD level. The geometrical parameters for the global minimum (which is found to be an open-chain *trans*-like isomer with the proton attached to a terminal oxygen atom, that is with a connectivity O_1–O_2–O_3–H^+) are as follows, with the B3LYP/cc-pVTZ values in parentheses: $r(O_1–O_2) = 1.200$ (1.170) Å; $r(O_2–O_3) = 1.403$ (1.404) Å; $r(O_3–H) = 0.994$ (0.993) Å; $\angle(O_1–O_2–O_3) = 112.8$ (114.0)°; $\angle(O_2–O_3–H) = 101.2$ (101.8)°. The corresponding *cis*-isomer is found to lie 3.6 and 3.5 kcal mol^{-1} above the global minimum at the B3LYP and CCSD(T) level of theory, respectively. The theoretical methods employed in the present work provide also a good agreement with experimental energetic information. For example, the predicted value for the ozone 300 K proton affinity at the B3LYP/cc-pVTZ and CCSD(T)/cc-pVTZ levels is 148.2 kcal mol^{-1}, whereas the experimental value obtained by Cacace and Speranza [3] is 148 ± 3 kcal mol^{-1}. At the same time the CCSD(T)/cc-pVTZ//B3LYP/cc-pVTZ ozone first ionization energy results as large as 12.50 eV in good agreement with experimental value of 12.53 eV. In the case of the proton affinity of CO the theoretical estimates at the B3LYP/cc-pVTZ and CCSD(T)/cc-pVTZ levels are 141.7 and 142.8 kcal mol^{-1}, respectively, whereas the experimental value is 142 kcal mol^{-1}.

The optimized geometries at the B3LYP/cc-pVTZ level of the most relevant intermediates in the reaction of $HO_3^+ + CO$ are shown in Fig. 1, whereas those for the transition states (TSs) are given in Fig. 2.

The vibrational frequencies and rotational constants for the intermediates and TSs are collected, respectively, in Tables 1 and 2. As can be seen in Table 1 all the intermediates are true minima on the PES, since all their vibrational frequencies are real. Finally, the relative energies of the possible products, intermediates and transition states are given in Table 3.

Intermediates I1–I4 are ion–molecule complexes (INCs) resulting from the interaction through the carbon atom of CO with the different sites of HO_3^+ and, although in qualitative terms, simple electrostatic arguments based on multipolar interaction can help in rationalizing the relative stability of these INCs. Let's consider, first of all, the partial charges on the ionic counterpart, i.e., protonated ozone. Their values at the

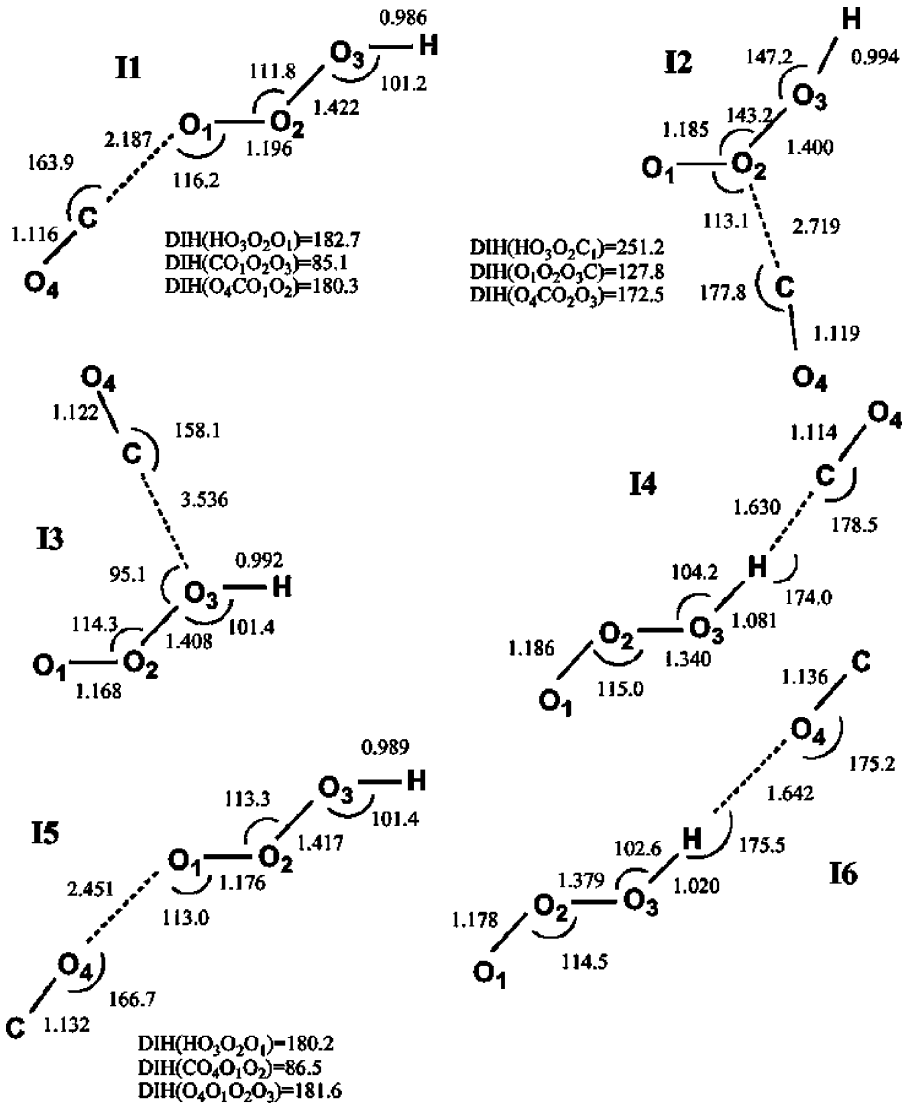

Fig. 1. B3LYP/cc-pVTZ optimized geometries for the more relevant intermediates in the reaction $HO_3^+ + CO$. Distances are given in angstroms (Å) and angles in degrees (°).

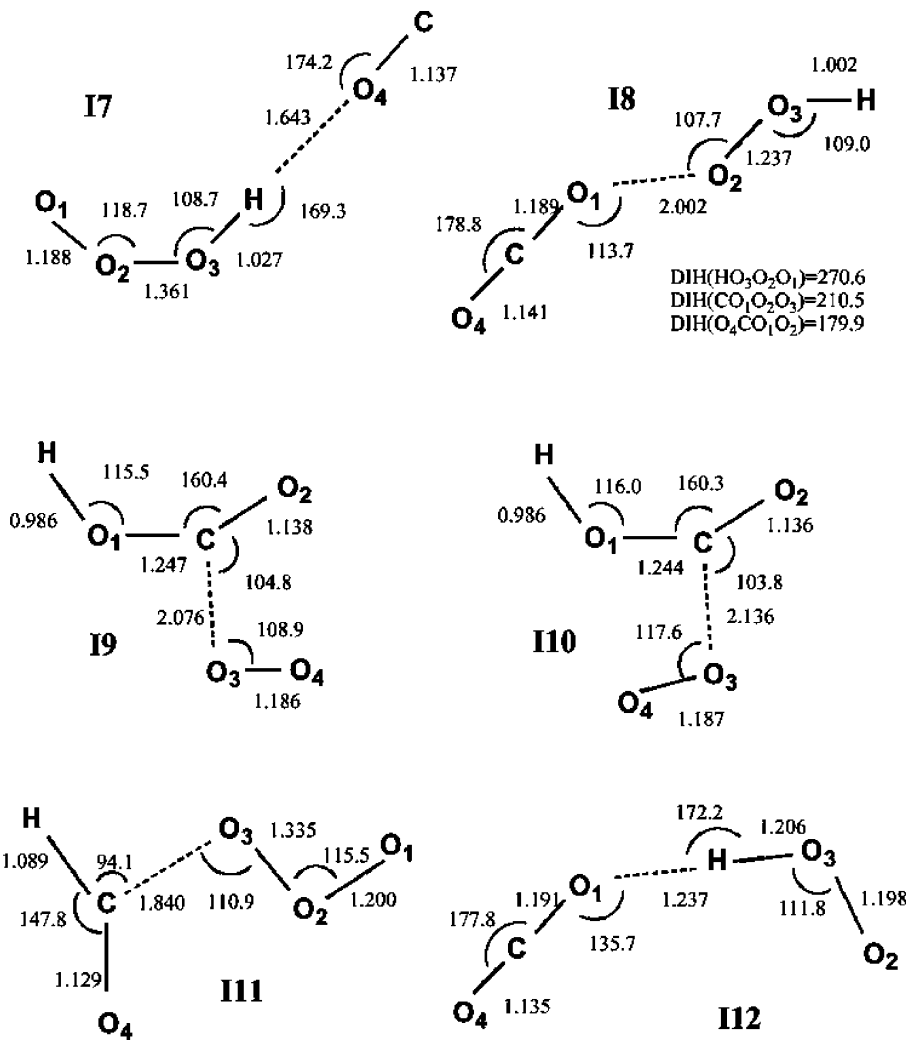

Fig. 1. (*Continued*).

coupled cluster level of theory, result to be equal to +0.315, +0.349, −0.002 and +0.338 a.u. for O_1, O_2, O_3 and H, respectively. The same level of theory describes the permanent dipole moment pointing toward the oxygen atom in the carbon monoxide and toward the hydrogen atom in the protonated ozone. Finally the calculated polarizability for carbon monoxide tensor shows the highest component along the internuclear axis. These calculated properties allow to carry out a detailed, although only indicative interpretation of the relative energies of the INCs. Such analysis strongly suggests that the dipole-induced dipole interaction plays a crucial role.

In fact, if we address the problem only in terms of pure charge–dipole interaction the best energetic situation would be expected for the I1, I2 and I4 INCs. For the same reason the I3 species would be essentially unbound and the I6, I7 and I5 INCs should represent unstable complexes. Similarly, if only the dipole–dipole interactions are considered, only in correspondence of

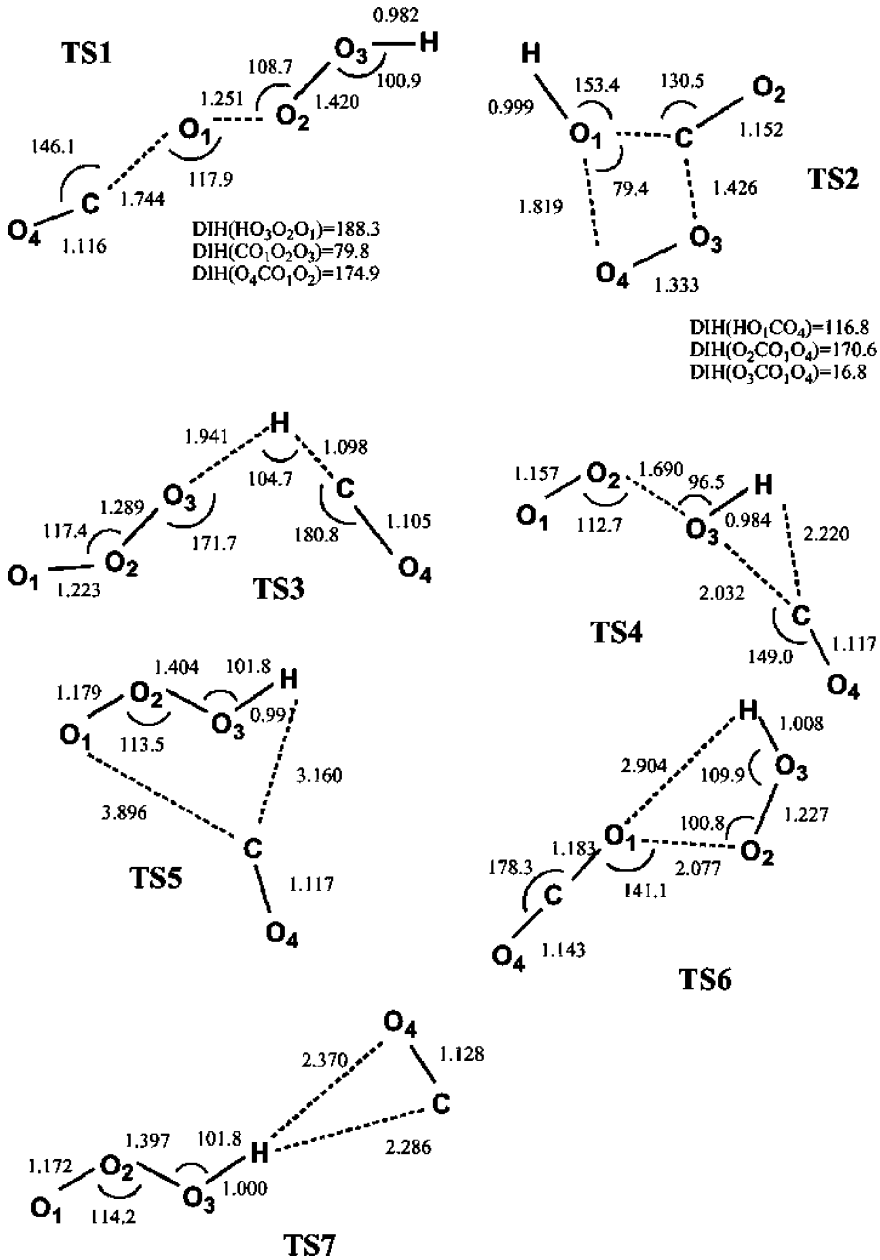

Fig. 2. B3LYP/cc-pVTZ optimized geometries for the transition states involved in the reaction $HO_3^+ + CO$. Distances are given in angstroms (Å) and angles in degrees (°).

I4 and I5 we would expect a stable situation whereas the I3 and I2 INCs should not provide bound states and all the other complexes should virtually not reside in energy minima. Only introducing the polarization effect in the carbon monoxide, all the connectivities able to maximize the dipolar interactions, i.e., all the INCs with the only exception of I3 and I2, can be expected to correspond to bound states. In the light of

Table 1
Vibrational frequencies (cm^{-1}) and rotational constants (GHz) for the relevant minima on the $(CO_4H)^+$ surface at the B3LYP/cc-pVTZ level

	I1	I2	I3	I4	I5	I6	I7	I8	I9	I10	I11	I12
Vibrational frequencies	84	80	43	86	51	67	70	50	115	75	116	26
	119	110	70	127	95	92	100	112	171	153	119	69
	153	119	88	227	99	128	126	224	209	195	156	219
	229	153	92	232	135	156	189	388	380	342	240	466
	401	245	145	264	197	216	224	630	426	410	538	619
	521	576	598	697	558	671	631	658	514	469	721	634
	622	594	616	905	614	852	871	681	594	586	901	842
	834	836	828	1079	821	876	927	1313	1109	1097	929	1104
	1322	1353	1366	1397	1356	1411	1407	1363	1227	1220	1127	1351
	1480	1522	1603	1588	1545	1596	1527	1506	1640	1635	1436	1524
	2288	2266	2246	2063	2151	2128	2124	2335	2294	2318	2106	1607
	3565	3445	3487	2324	3523	2976	2878	3308	3531	3530	3192	2457
A	16.848	11.657	12.440	39.851	16.039	37.521	14.274	28.263	10.261	10.337	21.009	21.101
B	2.116	1.999	15.946	1.488	2.064	1.640	2.148	2.218	3.949	3.709	2.857	1.858
C	1.995	1.743	1.413	1.434	1.892	1.571	1.867	2.100	2.852	2.730	2.515	1.708

Table 2
Vibrational frequencies (cm^{-1}) and rotational constants (GHz) for the relevant transition states in the reaction $O_3H^+ + CO$ at the B3LYP/cc-pVTZ level

	TS1	TS2	TS3	TS4	TS5	TS6
Vibrational frequencies	329i	734i	91i	365i	71i	49i
	89	232	43	97	83	75
	175	461	101	109	96	206
	265	532	105	229	110	311
	389	620	289	249	150	591
	541	709	724	346	572	623
	636	806	789	432	620	670
	880	957	877	617	827	1336
	1158	1071	1085	1185	1349	1395
	1445	1159	1341	1683	1548	1504
	2269	2021	2233	2276	2258	2344
	3601	3482	3136	3610	3506	3234
A	18.285	12.573	51.839	29.153	13.763	40.645
B	2.621	5.399	1.542	1.657	1.676	1.93
C	2.383	3.856	1.497	1.568	1.533	1.871

these consideration is therefore clear why I4, in correspondence of which each term of the multipolar interaction is attractive, represents the most stable species. However, only introducing the polarization effects we can explain the high stability of I6 and the not negligible interaction energy for the complexes I5 and I3. Obviously there is still something missing. Why does the I2 INC represent the less stable one? In order to address this question let's consider the difference between the I7 structure and I6. Basically they differ for the *trans*- to *cis*-isomerization of the ionic partner. As a matter of the fact their energy difference basically reflects the *cis–trans* energy gap, as described above. The same holds true for I2 and I3. But the *cis–trans* energy gap in the protonated ozone moiety is large enough to strongly destabilize the I2 species which, effectively, represents the less stable structure.

A general feature observed for these INCs is that the HO_3^+ moiety remains quite unaltered when the interaction is through one of its oxygen atoms (I1, I2, I3, I5). On the other hand, when the interaction takes place through the hydrogen atom, a noticeable shortening of the O_2–O_3 bond distance occurs simultaneously to the lengthening of the O_3–H bond.

In order to understand the factor governing the kinetic aspects of the overall process, it is of primary importance to address the question as to whether the actual formation of the INCs I1–I7 are kinetically relevant steps, i.e., their evolution into the final products are efficient routes with respect to their back-dissociation. In this context, all the INCs leading to the C-connectivity, i.e., I1–4 as well as the O-connected proton bridged I6 do actually show, at the level of theory herein employed, a monotonically attractive surface without the presence of any transition structures. The potential energy associated to the path leading to the complex I5 results, on the other hand, to slightly increase. This qualitative observation suggests that if we also consider the centrifugal barrier associated to dynamical event of the collision, the cross section for the generation of I5 is virtually equal to zero. At the same time the loose INCs I2 and I3 did not result to be able to propagate the reaction through first-order saddle point lower than the entrance channel. As a consequence of the fact any trajectory leading to the above species I2, I3 and I5 can be expected to be always back-reflected to CO and HO_3^+. Differently, the presence of the relatively low energy transition structures TS7, TS5 and TS1 should allow the encounter complexes I6, I4 and I1 to evolve into the final products.

The rest of minima shown in Fig. 1 are secondary possible intermediates in the $HO_3^+ + CO$ reaction

Table 3
Relative energies (kcal mol^{-1}) at different levels of theory, including ZPVE corrections

	B3LYP			CCSD(T)/cc-pVTZ
	cc-pVDZ	cc-pVTZ	aug-cc-pVTZ	
Reactants				
$CO + HO_3^+$	0.0	0.0	0.0	0.0
Total energy (electronic + ZPVE) (a.u.)	−338.97013	−339.07786	−339.08220	−338.51132
Products				
$O_2(^3\Sigma_g) + CO_2H^+(^1A')$	−96.1	−95.8	−96.0	−86.1
$O_2(^1\Delta_g) + CO_2H^+(^1A')$	−56.8	−57.1	−57.5	−56.0
$O_2(^3\Sigma_g) + CO_2H + (^3A'')$	8.9	12.0	11.8	26.0
$CO_2(^1\Sigma_g) + O_2H + (^1A')$	−53.2	−53.8	−53.8	−52.6
$CO_2(^1\Sigma_g) + O_2H + (^3A'')$	−68.5	−69.2	−69.2	−58.8
$O_3(^1A_1) + HCO + (^1\Sigma)$	6.8	6.5	4.7	6.9
$O_3(^1A_1) + HOC + (^1\Sigma)$	43.6	43.3	41.4	44.2
Intermediates				
I1	−15.9	−13.5	−13.1	−5.3
I2	−4.2	−2.9	−2.6	−0.6
I3	−2.4	−1.9	−1.7	−2.4
I4	−19.5	−16.1	−15.4	−15.1
I5	−6.8	−5.5	−5.3	−2.8
I6	−10.7	−8.6	−8.1	−8.4
I7	−7.3	−5.2	−4.6	−5.1
I8	−75.9	−73.5	−72.4	−60.6
I9	−67.9	−65.5	−64.2	−60.0
I10	−65.5	−64.4	−63.9	−58.9
I11	−10.8	−7.9	−7.5	−3.2
I12	−81.2	−79.2	−78.6	−76.2
Transition states				
TS1 (I1 → I8)	−13.9	−11.7	−11.1	−2.6
TS2 (I8 → I10)	−16.6	−14.1	−13.8	−9.2
TS3 (I4 → I11)	−5.7	−4.0	−4.2	−2.0
TS4 (I4 → I9)	−5.3	−1.9	−1.5	+3.5
TS5 (I4 → I1)	−6.5	−5.1	−4.9	−3.3
TS6 (I8 → I12)	−73.1	−71.1	−70.4	−60.5

and are in general (with the exception of I11) much more stable than the primary ion–molecule complexes. All of them are precursors of the different possible products in the reaction. I8 corresponds to a $OCO\cdots OOH^+$ complex, whereas I9 and I10 are the *cis* and *trans* arrangements, respectively, for the $HOCO^+\cdots O_2$ complex. All three are relatively long-distance complexes. I11 corresponds to the $HCO^+\cdots O_3$ complex, and has a shorter $C\cdots O$ distance, and therefore its low stability is undoubtedly related to the endothermicity of the products $HCO^+ + O_3$ (see Table 3). Finally I12 is actually a proton-bridged complex between $HOCO^+$ and singlet O_2. Any attempt of locating the $OCO\cdots HO_2^+$ complex failed both at the B3LYP level of theory and using second order perturbation theory. I12 is the lowest-lying $(CO_4H)^+$ species studied in this work which was found to lead to the $O_2 + CO_2H^+$ products, also obtained from I9 and I10, whereas I8 generates the less exothermic $CO_2 + HO_2^+$ species.

3.2. Hypothesis on the mechanistic features

On the basis of the above results, pictorically summarized in the Fig. 3 we could outline the mechanistic picture reported in Scheme 1.

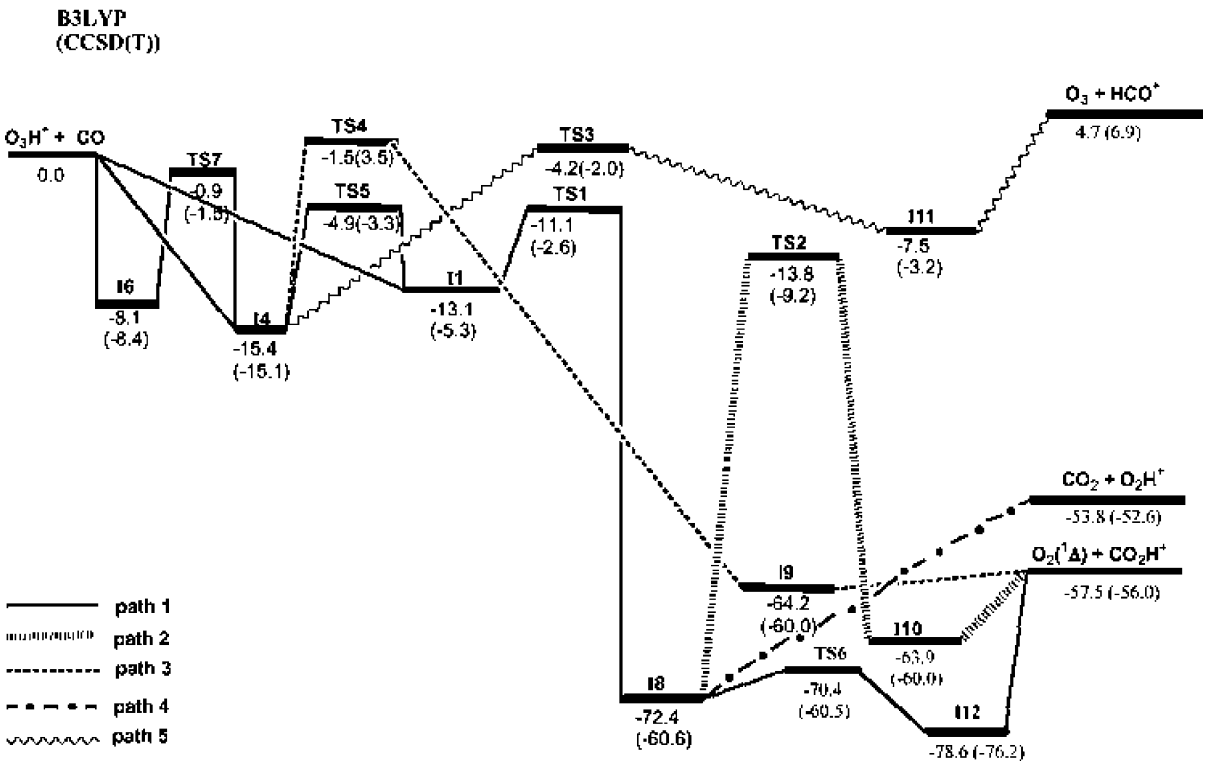

Fig. 3. B3LYP/aug-cc-pVTZ and CCSD(T)/cc-pVTZ (in parentheses) energy profile (in kcal mol^{-1}) for the reaction $HO_3^+ + CO$.

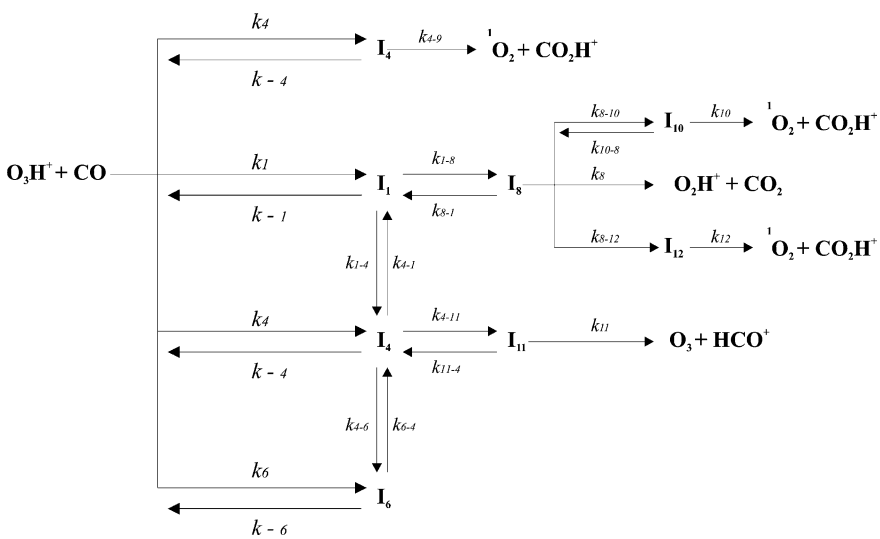

Scheme 1.

In this scheme we are assuming that only the INCs I1, I4 and I6 do play a mechanistic role. Moreover, we are also considering the strongly exothermic formation of the final precursors I8, I9, I10 and I12 as irreversible processes.

The above scheme shows five plausible paths. The first two respectively denoted as Path-1, i.e., INC-I8–I12-O_2/CO_2H^+, and Path-2, i.e., INC-I8–I10-O_2/CO_2H^+ essentially correspond to a two-step mechanisms. The first step, which is common to both of them, is characterized by the oxygen atom transfer to the CO moiety, i.e., formation of the I8 complex. The second step is characterized by the unimolecular intracomplex proton transfer from O_2 to CO_2 which is mechanistically different in the two paths. In Path-1 such proton transfer step takes place through a formal internal rotation of the HO_2^+ moiety which leads, through the transition structure TS6, directly to the proton bound dimer I12. On the other hand, in Path-2, the proton transfer occurs through the four-center transition structure TS2 forming the I10 complex.

A third reaction channel, which will be denoted as Path-3, i.e., INC-I9-O_2/HCO_2^+, clearly resembles a typical S_N2-like process.

The fourth reaction channel denoted as Path-4, i.e., INC-I8-CO_2/HO_2^+, represents an alternative evolution of the I8, i.e., its barrierless dissociation into CO_2 and HO_2^+. The last plausible route, i.e., Path-5, is the endothermic proton transfer from ozone to carbon monoxide generating O_3 and HCO^+ species. Such a channel, due to its endothermicity as large as about 7 kcal mol^{-1} at the coupled cluster level of theory, is not expected to generate any product in the typical low-pressure FT-ICR conditions which we are focussing on in the following kinetic analysis. Nevertheless, the same channel is not to be neglected by a mechanistic point of view. In fact, no high barriers are present along its path and therefore it is probably one of the events which lower the overall efficiency of the reaction (4).

3.3. Kinetic calculations

Both the formation of the encounter complexes I1–I6 and the dissociation of I8 to into HO_2^+ and CO_2, take place on monotonically attractive portions of the potential energy surface. Their kinetic treatment is therefore possible provided the corresponding transition states are variationally located along the above monotone portions of the surface. Both the RP and VRC-TST methods employed at this purpose virtually provided the same results and only the VRC-TST will be adopted hereafter. The following set of equations, from the steady-state treatment of all intermediates along the pathways, have been therefore obtained.

$$k_{\text{ov-1}}(T) = \frac{1}{hQ_r(T)}\sum_J (2J+1)\int_0^\infty [N_1(E,J)\cdot L(E,J)\cdot k_{8-12}(E,J) + N_4(E,J)\cdot G(E,J)\cdot k_{8-12}(E,J) + N_6(E,J)\cdot H(E,J)\cdot k_{8-12}(E,J)]\exp\left(-\frac{E}{kT}\right)\mathrm{d}E \quad (5)$$

$$k_{\text{ov-2}}(T) = \frac{1}{hQ_r(T)}\sum_J (2J+1)\int_0^\infty [N_1(E,J)\cdot L(E,J)\cdot k_{8-10}(E,J) + N_4(E,J)\cdot G(E,J)\cdot k_{8-10}(E,J) + N_6(E,J)\cdot H(E,J)\cdot k_{8-10}(E,J)]\exp\left(-\frac{E}{kT}\right)\mathrm{d}E \quad (6)$$

$$k_{\text{ov-3}}(T) = \frac{1}{hQ_r(T)}\sum_J (2J+1)\int_0^\infty \frac{k_{4-9}(E,J)}{D(E,J)}\left[\frac{N_1(E,J)\cdot k_{-1}(E,J)}{A(E,J)\cdot C(E,J)} + \frac{N_4(E,J)}{A(E,J)} + \frac{N_6(E,J)\cdot k_{6-4}(E,J)}{A(E,J)\cdot B(E,J)}\right]\exp\left(-\frac{E}{kT}\right)\mathrm{d}E \quad (7)$$

$$k_{\text{ov-4}}(T) = \frac{1}{hQ_r(T)} \sum_J (2J+1) \int_0^\infty [N_1(E,J) \cdot L(E,J) \cdot k_{d8}(E,J) + N_4(E,J) \cdot G(E,J) \cdot k_{d8}(E,J) + N_6(E,J) \cdot H(E,J) \cdot k_{d8}(E,J)] \exp\left(-\frac{E}{kT}\right) dE \quad (8)$$

$k_{\text{ov-1}}(T)$, $k_{\text{ov-2}}(T)$, $k_{\text{ov-3}}(T)$ and $k_{\text{ov-4}}(T)$ are the thermally averaged rate constants, in the ideal gas approximation, concerning the Path-1, Path-2, Path-3 and Path-4, respectively. Their summation provides, obviously, the global phenomenological rate constant for the process (4). $Q_r(T)$ are the molecular partition functions of the reactants in the center of the mass frame and k is the Boltzmann constant.

In the above equations:

$$A(E,J) = k_{-4}(E,J) + k_{4-6}(E,J) + k_{TS4}(E,J) + k_{-11}(E,J)$$

$$B(E,J) = k_{6-4}(E,J) + k_{-6}(E,J)$$

$$C(E,J) = k_{1-8}(E,J) + k_{-1}(E,J) + k_{1-4}(E,J)$$

$$D(E,J) = \frac{k_{6-4}(E,J)k_{4-6}(E,J)}{A(E,J)B(E,J)} + \frac{k_{-1}(E,J)k_{4-1}(E,J)}{A(E,J)C(E,J)} + \frac{k_{4-11}(E,J)}{A(E,J)}$$

$$F(E,J) = \frac{k_4(E,J)}{A(E,J)} + \frac{k_{6-4}(E,J)k_6(E,J)}{A(E,J)B(E,J)} + \frac{k_1(E,J)k_{-1}(E,J)}{A(E,J)C(E,J)}$$

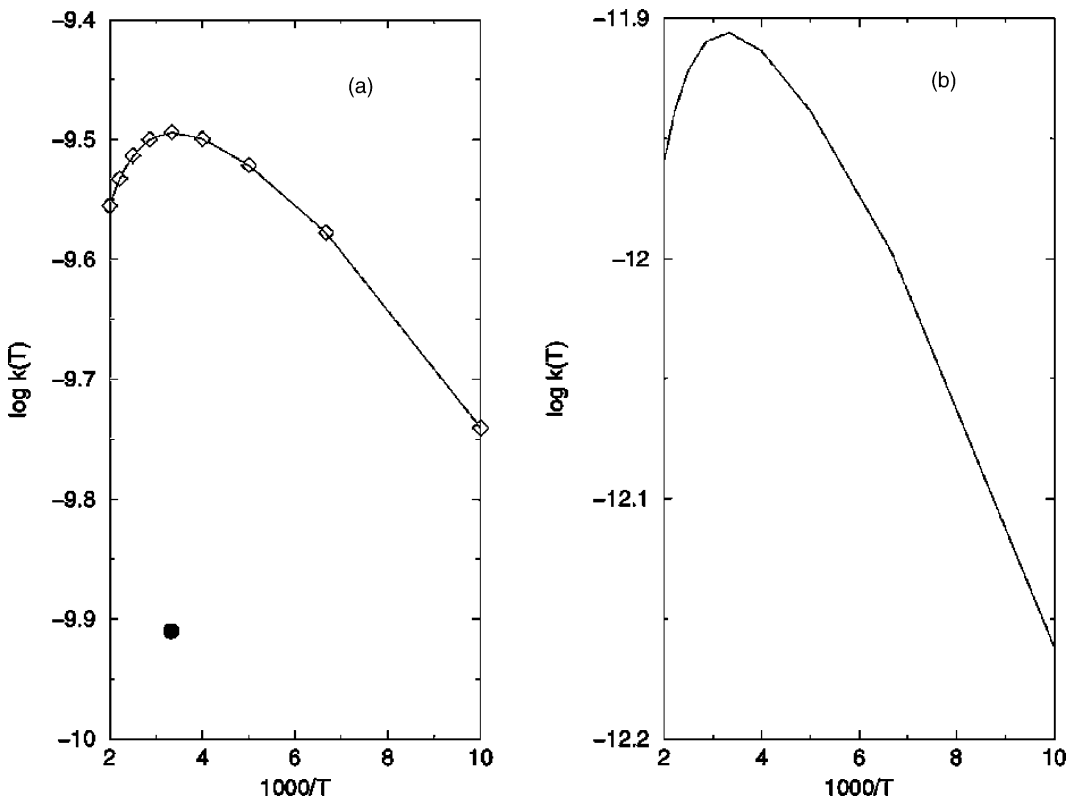

Fig. 4. (a) Arrhenius plot of the overall rate constants for the channel leading to O_2 and HCO_2^+ (Path-1 + Path-2 + Path-3, solid line and Path-1, diamonds). (b) Arrhenius plot of the overall rate constant for the channel leading to HO_2^+ and CO_2, i.e., Path-4. Units are in K for the temperatures and $cm^3\,molecule^{-1}\,s^{-1}$ for the rate constants.

$$G(E,J) = \frac{k_{1-8}(E,J)}{A(E,J)D(E,J)(k_{d8}(E,J) + k_{8-12}(E,J))}$$

$$L(E,J) = \frac{k_{1-8}(E,J)}{C(E,J)(k_{d8}(E,J) + k_{8-12}(E,J))} + \frac{k_{1-8}(E,J)k_{-1}(E,J)}{A(E,J)C(E,J)D(E,J)(k_8(E,J) + k_{8-12}(E,J))}$$

$$H(E,J) = \frac{k_{6-4}(E,J)k_{1-8}(E,J)}{A(E,J)B(E,J)D(E,J)(k_{d8}(E,J) + k_{8-12}(E,J))}$$

The results are collected in Fig. 4. In this figure we have separately reported the Arrhenius plot concerning the formation of the O_2/CO_2H^+, i.e., the sum of the $k_{ov\text{-}1}(T)$, $k_{ov\text{-}2}(T)$ and $k_{ov\text{-}3}(T)$ in panel a, and concerning the formation of O_2/CO_2H^+, i.e., $k_{ov\text{-}4}(T)$ in panel b.

In the panel a we also report, through the diamonds, the values of the thermal rate constant $k_{ov\text{-}1}(T)$ referred only to the Path-1 which clearly represents the only route kinetically open for the formation of singlet oxygen and protonated carbon dioxide. Moreover, these products turn out to be the only plausible reaction products. In fact, by comparing the panel b and the panel a, the value of $k_{ov\text{-}4}(T)$, i.e., the rate constant for the channel leading to the alternative O_2/CO_2H^+ products, is more than 100 times smaller than the $k_{ov\text{-}1}(T)$.

It is also to be remarked the non-linear temperature dependence of the overall rate constant. Such a behavior is rather usual for bimolecular reactions in vacuo. At low temperatures in fact, where the rate coefficient is basically dominated by enthalpic activation factors, a positive trend is observed. On the other hand, when the temperature is increased and the overall reaction is governed by activation entropy, the trend becomes negative.

In the same panel a we also report with a full circle, the experimentally FT-ICR measured rate constant at 300 K. By comparing the experimental result (1.2×10^{-10} cm^3 molecule^{-1} s^{-1}) with the presently calculated rate constants at 300 K (3.0×10^{-10} cm^3 molecule^{-1} s^{-1}) the following considerations can be drawn: first, the agreement is rather good for what concerns the absolute value of the rate constant. Second, the nature of the generated products, i.e., basically only O_2 and HCO_2^+, fully fits the experimental observation [4].

The success of the first result is probably to be ascribed to the adequacy of the statistical models in describing in the present case the kinetically relevant steps, i.e., the formation and evolution of the active encounter complexes. Such a correct description probably comes out from the fact that the formation of I1, I4 and I6 are relatively slow events allowing an efficient randomization of the internal energy of the complexes. Much more complicated is the attempt of explaining the success in reproducing the exclusive formation of the experimentally observed products. In terms of statistical rate theories our results suggest that the larger contribution of the Path-1 can be ascribed to the dimensions of the phase-space volume associated to the TS6 resulting systematically larger, at the sampled energies and angular momenta, than the phase-space volume of the variational TSs along the I8 dissociation path. This is in fact shown in the Fig. 5 where we compare the microcanonical rate coefficients for the interconversion of I8–I12, in solid line, and the microcanonical rate coefficients for the barrierless dissociation of I8 in dashed line. We report the above coefficients at four different values of J, i.e., 0, 20, 30 and 60. It can be observed that for all the values of J, if we disregard high values of energies actually not sampled at the temperatures of interest, the barrierless reaction for the formation of HO_2^+ and CO_2 never appears to efficiently compete. However, several authors [22] including ourselves [23] have pointed out that a typical impulsive process, similar to the one expected to characterize both the formation of I8 and its evolution into the products, shows a behavior very far from being statistical. In such very fast processes the volume of the phase space effectively sampled along the trajectory usually represents only a small portion of the one actually available. Rather, the extent of the coupling of the internal degrees of freedom with the reaction coordinate does generally govern the dynamical event and, therefore, the ‘choice’ of the path. In the present

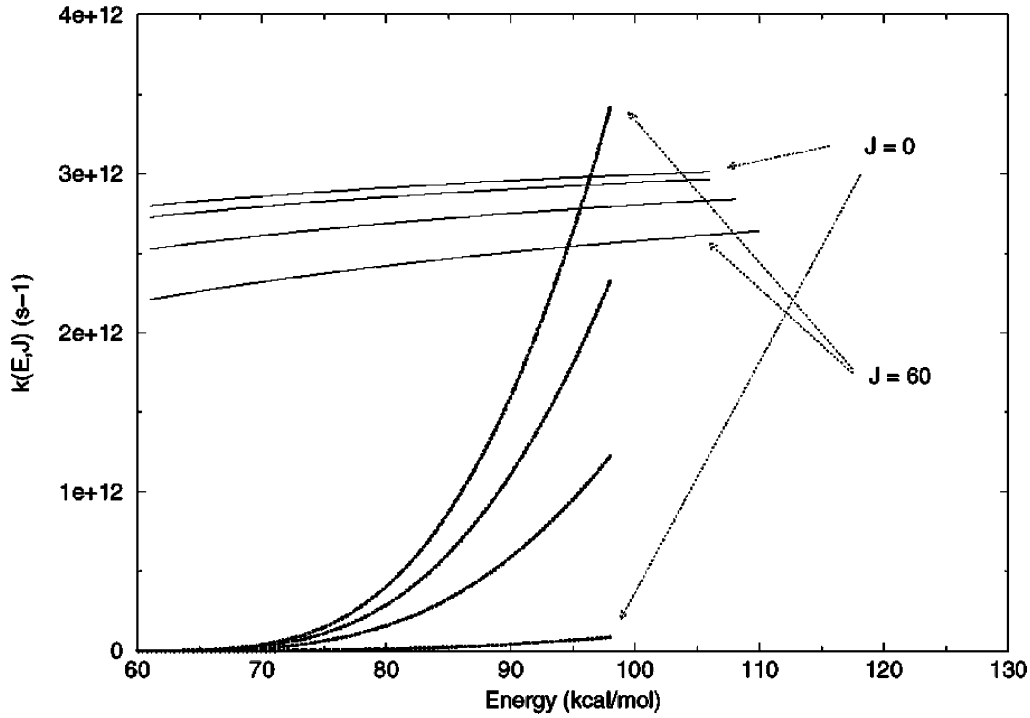

Fig. 5. Comparison between the microcanonical rate coefficients for the I8-TS6-I12 (solid line) and I8-CO_2/HO_2^+ (dashed line). The curves have been reported at four different values of the total angular momentum J (0, 20, 30, 60) whose lower (0) and upper (60) limits are indicated with arrows. The zero of the energy corresponds to the reactants energy (see Fig. 3).

case the question is open as to whether our system is effectively non-RRKM behaved with a fortuitous coincidence of the nature of the products or, alternatively, its ability in redistributing the internal energy is so high to ensure a statistical behavior. Of course other experimental data such as measurements of rate coefficients at different temperatures or the analysis of the products energy distribution would greatly help in answer the above question which, however, should be grounded on a more explicitly dynamical approach [23].

4. Conclusions

The oxidation reaction of carbon monoxide promoted by protonated ozone turns out, from quantum-chemical calculations, to be a bimolecular reaction much more complicated than a simple nucleophilic substitution over the OH^+ moiety. The reaction is obviously initiated with the formation of the HO_3^+/CO encounter complexes. Their lifetime, at least in the range of energy and angular momentum sampled in this work, resulted not long enough to allow an efficient propagation of the reaction which, however, proceeds through a two-step mechanism in which the oxygen and hydrogen atoms are successively transferred from the protonated ozone to the carbon monoxide. The 300 K experimental results, i.e., the rate constant equal to 1.2×10^{-10} cm^3 molecule^{-1} s^{-1} and the specificity of the reaction products, i.e., O_2 and HCO_2^+, are reproduced with a satisfactory agreement. The possibility of a parallel reaction route characterized by spin-crossing is also to be taken into account although its explicit analysis will be addressed in a forthcoming paper.

Acknowledgements

This research has been supported by the Ministerio de Ciencia y Tecnologia of Spain (DGICYT, Grant BQU2001-3660-C02-02), by the Junta de Castilla y León (Grant VA 18/00B) and by *Fondi di Rilevante Interesse di Ateneo* University of l'Aquila. M.A. would like to thank Prof. Maurizio Speranza for helpful discussions, Prof. Alfredo Di Nola for the computational facilities at the CASPUR-Rome, and Mr. Renato Di Bartolomeo for his help in the preparation of the manuscript.

References

[1] N. Yoneda, G.L. Olah, J. Am. Chem. Soc. 99 (1977) 3113.
[2] (a) M. Kausch, P.R. Schleyer, J. Comput. Chem. 1 (1980) 94; (b) C. Meredith, G.E. Quelch, H.F. Schaefer III, J. Am. Chem. Soc. 113 (1991) 1186; (c) I.I. Zacharov, O.I. Kolbasina, T.N. Semenyuk, N. Tyupalo, G.M. Zhidomirov, Zh. Struct. Khim. 34 (1993) 28.
[3] F. Cacace, M. Speranza, Science 265 (1994) 208.
[4] M. Speranza, Inorg. Chem. 35 (1996) 6140.
[5] B.R. Rowe, D.W. Fahey, E.E. Ferguson, F.C. Feshenfeld, J. Chem. Phys. 75 (1981) 3325.
[6] T. Su, M. Bowers, in: M. Bowers (Ed.), Gas Phase Ion Chemistry, vol. 1, Academic Press, New York, 1979.
[7] S.G. Lias, J.A. Barmess, J.F. Liebman, J.L. Holmes, R.D. Levin, W.G. Mallard, J. Phys. Chem. Ref. Data 17 (Suppl. 1) (1988).
[8] A.D. Becke, J. Chem. Phys. 98 (1993) 5648.
[9] C. Lee, W. Yang, R.G. Parr, Phys. Rev. B 37 (1988) 785.
[10] T.H. Dunning, J. Chem. Phys. 90 (1989) 1007.
[11] D.E. Woon, T.H. Dunning, J. Chem. Phys. 98 (1993) 1358.
[12] K. Raghavachari, G.W. Trucks, J.A. Pople, M. Head-Gordon, Chem. Phys. Lett. 157 (1989) 479.
[13] M.J. Frisch, G.W. Trucks, H.B. Schlegel, G.E. Scuseria, M.A. Robb, J.R. Cheeseman, V.G. Zakrzewski, J.A. Montgomery, Jr., R.E. Stratmann, J.C. Burant, S. Dapprich, J.M. Millan, A.D. Daniels, K.N. Kudin, M.C. Strain, O. Farkas, J. Tomasi, V. Barone, M. Cossi, R. Cammi, B. Mennucci, C. Pomelly, C. Adamo, S. Clifford, J. Ochterski, G.A. Petersson, P.Y. Ayala, Q. Cui, K. Morokuma, D.K. Malick, A.D. Rabuck, K. Raghavachari, J.B. Foresman, J. Cioslowski, J.V. Ortiz, A.G. Baboul, B.B. Stefanov, G. Liu, A. Liashenko, P. Piskorz, I. Komaromi, R. Gomperts, R.L. Martin, D.J. Fox, T. Keith, M.A. Al-Laham, C.Y. Peng, A. Nanayakkara, C. Gonzalez, M. Challacombe, P.M.W. Gill, B. Johnson, W. Chen, M.W. Wong, J.L.M. Head-Gordon, E.S. Replogle, J.A. Pople, Gaussian 98, Gaussian Inc., Pittsburgh, PA, 1998.
[14] D.G. Truhlar, B.C. Garrett, S.J. Klippenstein, J. Phys. Chem. 100 (1996) 12771.
[15] E.E. Aubanel, D.M. Wardlaw, L. Zhu, W.L. Hase, Int. Rev. Phys. Chem. 10 (1991) 249.
[16] W.H. Miller, N.C. Handy, J.E. Adams, J. Chem. Phys. 72 (1980) 99.
[17] S.J. Klippenstein, Chem. Phys. Lett. 170 (1990) 71.
[18] S.J. Klippenstein, A.F. Wagner, R.C. Dunbar, D.M. Wardlaw, S.H. Robertson, VARIFLEX: Version 1.00, July 16, 1999.
[19] P.J. Robinson, K.A. Holbrook, Unimolecular Reactions Wiley/Interscience, London, 1971.
[20] W.H. Miller, J. Am. Chem. Soc. 101 (1979) 6810.
[21] M. Ceotto, F.A. Gianturco, J. Phys. Chem. A 103 (1999) 9984.
[22] T. Baer, W.L. Hase, Unimolecular Reaction Dynamics. Theory and Experiments, Oxford University Press, Oxford, 1996, p. 361, and references reported therein.
[23] M. Aschi, F. Grandinetti, Eur. J. Mass Spectrom. 6 (1999) 31.